Since January 2020 Elsevier has created a COVID-19 resource centre with free information in English and Mandarin on the novel coronavirus COVID-19. The COVID-19 resource centre is hosted on Elsevier Connect, the company's public news and information website.

Polymer 222 (2021) 123643

Contents lists available at ScienceDirect

Polymer

journal homepage: http://www.elsevier.com/locate/polymer

Engineering laminated paper for SARS-CoV-2 medical gowns

Laila Hossain [a,b,1], Maisha Maliha [a,b,1], Ruth Barajas-Ledesma [a,b,1], Jinhee Kim [b], Kevin Putera [b], Dinesh Subedi [c], Joanne Tanner [a,b], Jeremy J. Barr [c], Mark M. Banaszak Holl [b], Gil Garnier [a,b,*]

[a] Bioresource Processing Research Institute of Australia (BioPRIA), Australia
[b] Department of Chemical Engineering, Monash University, VIC, 3800, Australia
[c] School of Biological Sciences, Monash University, VIC, 3800, Australia

ARTICLE INFO

Keywords:
Medical gown
Virus protection
Barrier material
PE laminated Paper
COVID-19
Coating morphology

ABSTRACT

The COVID-19 pandemic has highlighted the need for diversity in the market and alternative materials for personal protective equipment (PPE). Paper has high coatability for tunable barrier performance, and an agile production process, making it a potential substitute for polyolefin-derived PPE materials. Bleached and newsprint papers were laminated with polyethylene (PE) coatings of different thicknesses, and characterised for their potential use as medical gowns for healthcare workers and COVID-19 patients. Thicker PE lamination improved coating homogeneity and water vapour resistance. 49 GSM bleached paper with 16 GSM PE coating showed high tensile and seam strength, and low water vapour transmission rate (WVTR). Phi-X174 bacteriophage testing revealed that paper laminated with 15 GSM coating hinders virus penetration. This research demonstrates that PE laminated paper is a promising material for low cost viral protective gowns.

1. Introduction

In March 2020, the World Health Organisation declared the outbreak of COVID-19 to be a global pandemic. The highly infectious nature of the virus SARS-CoV-2, which causes COVID-19, has made the prevention of person-to-person transmission a critical mechanism to halt the spread of the disease. The use of personal protective equipment (PPE) is therefore vitally important [1]. Without appropriate protection from exposure to the SARS-CoV-2 virus, front-line health care workers are at great personal risk, and represent a critical transmission link to other patients and their families [2]. The rapid spread of COVID-19 and the consequential increase in demand for PPE has resulted in significant worldwide PPE shortages, including medical gowns.

Medical gowns are designed to prevent the transmission of pathogens to the wearer from an infected patient's body fluids [3,4]. These have been shown to be superior to apron-style coverings in the reduction of contamination from splashes [5,6]. According to the American Food, Drug and Cosmetic act [7], PPE used in healthcare facilities is considered to be a medical device. PPE is categorised as either a Class I (low to moderate risk) or Class II (moderate to high risk) device by the USFDA [8]. Medical gowns are classified as Class II medical devices, for which regulatory standards must be met for commercialisation [9]. According to the AAMI PB70 standard, the four tests required for the barrier performance of medical gowns are water, hydrostatic pressure, blood penetration and virus penetration resistance [10]. Based on their performance in these tests, medical gowns are categorised from level 1 (low protection) to level 4 (high protection) [11].

In the absence of genuine and appropriate PPE, many workers have been forced to adopt makeshift solutions, such as wearing plastic garbage bags as gowns, which do not meet any of the above standards [12]. Public Health England sought to mitigate the shortage of appropriate PPE by allowing the use of reusable laboratory coats and patient gowns made of washable, woven fabrics as alternatives to disposable, non-woven gowns [13]. Many PPE manufacturers have increased or introduced the production of reusable gowns to meet the increasing demand [14–16]. However, some products only meet level 2 [17] or level 3 [18] regulatory requirements. Granzow [19] demonstrated that reusable woven fabric gowns have a lower resistance to microorganism and liquid penetration than disposable non-woven polypropylene gowns, which achieve the best liquid penetration resistance.

The global pandemic, spike in demand, and shortage of traditional PPE materials suitable for viral transmission protection has driven biopolymer researchers, virologists, and biomedical experts to collaborate and explore low cost alternative materials for medical gowns and

* Corresponding author. Bioresource Processing Research Institute of Australia (BioPRIA), Australia.
E-mail address: gil.garnier@monash.edu (G. Garnier).
[1] Authors contribute equally.

https://doi.org/10.1016/j.polymer.2021.123643
Received 9 November 2020; Received in revised form 3 March 2021; Accepted 12 March 2021
Available online 19 March 2021
0032-3861/

other PPE [20]. Laminated paper is a non-woven material with significant potential for use as medical gowns. The inherent properties, ubiquitous availability, low cost, and agile paper production and lamination processes make this material widely available, suitable to address the health-care criteria, and able to adapt to rapid changes in demand during a pandemic event or other emergency that results in critical PPE shortage situations. Laminated paper materials are attracting attention for their physical properties, as well as their renewability and biodegradability in many industries including packaging [21–23], superabsorbents [24–27], membranes [28,29] and biomedical [30–32]. However, the use of paper-based protective apparel has not yet been reported.

This study presents engineered and optimised laminated paper composite materials for medical gowns. Paper as the base material provides the mechanical strength, and a thin laminated coating of polyethylene acts as a barrier to increase the level of viral protection of the gowns. The effects of basis weight, laminate thickness, and combinations thereof on the composite performance were determined. The mechanical and barrier properties, viral protection, and liquid resistance of the composites were quantified. The ease of gown manufacture and performance with respect to the regulatory requirements for Level 4 medical gowns were critically evaluated. Finally, bespoke prototypes were designed and manufactured from the optimised laminated paper material, and feedback from health-care workers was sought to demonstrate the application.

2. Methodology

2.1. Materials

Polyethylene was provided by Qenos Pty Ltd. Machine glazed bleached eucalyptus paper and newsprint paper were provided by Opal, Maryvale, VIC, Australia (formerly known as Australian Paper) and Norske Skog Boyer, Australia, respectively. Anhydrous calcium chloride was purchased from Sigma Aldrich. The surfactant polysorbate 80 was purchased from Sigma-Aldrich, Australia. Whatman filter paper 602H was obtained from Bio-Strategy Pty limited Australia.

2.2. Preparation of laminated paper

The base sheets were coated on one or two sides with a blend of low density polyethylene (LDPE) and linear low-density polyethylene (LLDPE), referred to simply as polyethylene (PE) in this paper. Paper samples were coated at Opal Specialty Paper, VIC, Australia (formerly known as Orora) by extrusion coating. In this process, polyethylene is melted at high temperature (300 °C to 320 °C) and pressure, extruded through a slit die and laminated onto a paper substrate at high temperature through a nip roll assembly. The nip roll assembly consists of a rubber-covered pressure roll and water-cooled chill roll. The paper is fed from the rubber-covered pressure roll into the nip where lamination is achieved by pressing the polyethylene and paper layer together. The formed laminate is rapidly cooled down by water-cooled chill roll (15 °C to 30 °C) and collected by a wind-up mechanism. The sample description and composition is given in Table 1.

2.3. Sample thickness

The thickness of the material was measured using the L&W Micrometer (model no. 222). The sample thickness was calculated as the average of 5 random points for 5 replicates.

2.4. Coating defect analysis

2.4.1. Fluorescence and optical imaging

Fluorescence staining was employed to detect defects in the PE coating, followed by optical microscopy in transmission and reflectance mode to visualise the overall coating morphology. In theory, the fluorescence dye should stain defects on PE coating if the nature of the defect is a hole in the coating that exposes the underlying paper. Diluted propidium iodide (PI) solution was prepared by mixing 20 μL of stock solution (10 mM) with 80 μL of deionised water, then passing through a 0.2 μm syringe filter before spraying the solution onto the coated side(s) of the sample. PI droplets on the coated surface were dried by wicking with a delicate task wipe (Kimwipe), and the surface was rinsed with deionised water to remove any residue on the coated surface before a final drying with Kimwipe. Fluorescence images of the pinhole structures were taken with the PE coated side up using a Nikon upright microscope (model DS-Ri2) employing a TRITC filter (Ex 540/24, DM 565, BA 605/55) with 10x objective lens. The entire surface was scanned before capturing images of the location(s) with the largest observed pinholes. Pinhole defects appeared as red spots on the sample during fluorescence imaging. Pinholes were not always visible in the optical images. Transmission (brightfield) and reflectance images were captured sequentially at the same location using the same microscope. Reflectance images were captured with a coloured filter to enhance contrast. A fine tipped marker was used to circle the pinhole location on the PE coating to direct the subsequent acquisition of topography and chemical composition information with AFM-IR.

2.4.2. Atomic force microscopy – infrared spectroscopy (AFM-IR)

The AFM-IR data were collected with a Bruker NanoIR3 system. AFM images of pinholes identified during fluorescence and optical imaging were captured areas of 3 × 3 μm to 30 × 30 μm at 0.7Hz line scan rate with 100–200 pixel density on each edge using contact mode probes (Model: PR-EX-nIR2-10). Two to four height images were stitched together depending on the defect size in order to visualise the defect topography. Four IR spectra within the range 790–1850 cm^{-1} were taken at locations of interest with 18.74% laser power, 2.9% duty cycle, and 2429 pt IR focus spot. The resonant frequency of the tip was tuned to around 265 kHz. IR imaging was performed with IR peaks unique to PE and cellulose – 1464 cm^{-1} and 1062 cm^{-1}, attributed to CH_2 wag and C–O stretch, respectively – to acquire IR maps of the PE-to-cellulose ratio on the coated surface.

2.5. Mechanical properties

2.5.1. Tensile strength

Bare and laminated paper samples were tested for tensile strength in accordance with the TAPPI T402 standard using an Instron tensile tester

Table 1
Description and composition of laminated paper materials examined in this study.

Sample code	Sample Details	
	Base sheet	Laminate
N42/10	Newsprint 42 GSM	Polyethylene 10 GSM
N51/10	Newsprint 51 GSM	Polyethylene 10 GSM
B44/0	Bleached 44 GSM	–
B44/6	Bleached 44 GSM	Polyethylene 6 GSM
B44/10	Bleached 44 GSM	Polyethylene 10 GSM
B44/15	Bleached 44 GSM	Polyethylene 15 GSM
B49/0	Bleached 49 GSM	–
B49/16	Bleached 49 GSM	Polyethylene 16 GSM
15/B49/16	Bleached 49 GSM	Double side coated with Polyethylene 15 GSM and 16 GSM

(model 5965). The samples were cut into 50 mm wide strips by laser cutter and tested at a constant strain rate of 10 mm/min. Five replicates were measured in each direction (machine direction: MD and cross direction: CD). Geometric mean tensile (GMT) was calculated by the square root of the product of the MD tensile load and CD tensile load at break.

$$\mathrm{GMT} = \sqrt{(\text{Tensile load at MD} \times \text{Tensile load at CD})}$$

2.5.2. Tear strength

Tear strength was measured following ASTM D5587-15. Rectangular samples of dimension 150 mm by 75 mm were cut by laser cutter (Epilog Laser). Following the standard, an isosceles trapezoid template of 25 mm by 102 mm was drawn for each sample. A preliminary cut 15 mm long was made at the centre of the 25 mm edge. Samples were tested using an Instron tensile tester (model 5965) at a constant strain rate of 300 mm/min. Five replicates were measured for each direction (machine direction: MD and cross direction: CD) and the arithmetic mean value is reported.

2.5.3. Seam strength

Seam strength was measured following ASTM D751-19. Rectangular samples with a dimension of 50 mm by 203 mm were cut by laser cutter (Epilog Laser). The sample was folded in half with the fold parallel to the short direction of the sample. The fold was sewn in a seam (stitch type: 301) approximately 100 mm from one end using a Janome N190 sewing machine with polyester thread (Gutermann 274 yds/vgs) and a denim needle (denim needle 16; 15 × 1DE). The fold was cut after seaming, and the samples unfolded at the seam or strength testing using an Instron tensile tester (model 5965) at a constant strain rate of 300 mm/min. Five replicates were measured for each direction (machine direction: MD and cross direction: CD) and the arithmetic mean value is reported. For thermofused samples, the samples were folded similarly as described for sewn samples. Then the samples were cut through the fold and thermofused by a heat sealer (Sunbeam VAC 780).

2.5.4. Statistical analysis

The tensile and the seam strengths were analysed to determine the variance in the results from each type of sample, and to determine whether there were statistically significant differences between them. This was done using GraphPad Prism 8.0.2 by one-way analysis of variance (ANOVA) for the whole set of data, followed by Tukey's post hoc test to compare individual samples.

2.6. Barrier properties

2.6.1. Water penetration

Impact penetration tests were evaluated in triplicate following the standard AATCC TM42-2017e [33]. Samples and blotting papers were conditioned at 21 °C and 50% relative humidity for at least 4 h before testing. Once conditioned, each sample was clamped under a spring clamp located at the top of a stand with an inclination of 45°. Another spring clamp with a weigh of 0.5 kg was clamped at the free end of the sample. A previously weighed blotting paper was placed beneath the sample.

A funnel with a spray nozzle at the bottom was placed 0.6 m above the top of the inclined stand (measured from the middle). The nozzle had 25 holes of 1 mm diameter. 500 mL of deionised water was poured into the funnel and allowed to spray under gravity onto the sample. The weight of the blotter paper was measured immediately after the water spraying finished.

2.6.2. Hydrostatic pressure

Hydrostatic pressure tests were performed in triplicate using a set up adapted from the standard AATCC TM127-2018 [34]. Samples were conditioned at 21 °C and 50% relative humidity for at least 4 h before testing. A pre-fabricated polypropylene tube of 15 cm diameter and 100 cm height with two clear plaques at the bottom was used to conduct the tests. Each sample was inserted in between these plaques and tighten with screws. Deionised water was poured inside the tube with the sample at the bottom until leaks were observed. The height of the water in the tube was recorded.

2.6.3. Water vapour transmission rate

The water vapour transmission rate (WVTR) of the samples was measured using the desiccant method according to the standard ASTM E96. The samples were dried in an oven at 105 °C for at least 4 h prior to the test. Permeability cups containing pre-dried calcium chloride were sealed with the laminated side (outside surface) of the samples facing the desiccant, and the paper side (inside surface) facing the environment. The WVTR testing was conducted at 23 °C and 50% relative humidity. The change in mass of the cups with time was recorded and plotted. The slope of the rate of change of mass was used to calculate the water vapour transmission rate.

2.7. Virus protection

2.7.1. Preparation of phage suspension

Bacteriophage Phi-X174 was used in this assay as a model virus as it is non-pathogenic to humans. Phi-X174 was propagated using host *Escherichia coli* C ATCC 13706. The lysate was purified following the Phage-on-Tap protocol [35]. Chloroform extraction was not performed during phage purification of the lysate due to incompatibility with the test materials. The phage titre was determined by the soft agar overlay method, in which phage lysate was diluted 10 fold in bacteriophage nutrient broth [Bacto-tryptone (8.0 ± 0.1) g + Potassium chloride (5.0 ± 0.06) g + Calcium chloride (0.2 ± 0.003) g + Purified water (pH 5.3) (1 000 ± 12.5) ml] with surfactant [poly-sorbate 80 (0.1 ± 0.001 25) ml] to simulate the surface tension range for blood and body fluids.

2.7.2. Penetration test

The resistance of the material to Bacteriophage Phi-X174 was studied using the standard method ISO 16604:2004 (E). Herein, Phi-X174 in liquid was used in contact with the outside surface (laminated side) of the material. 90 mm diameter sample were tested in a penetration cell of diameter 70 mm. The penetration test cell and the samples were steam sterilised at 121 °C and 214 kPa for 15 min before each test. The sample was placed within the penetration cell, and the cell was closed by torqueing the bolts to 2.8 Nm each. The cell was covered with the transparent cover and mounted vertically in the apparatus for the penetration test. The cell was filled with 75 ± 2 mL of approximately 10^7 plaque forming units (pfu)/mL of Phi-X174 (challenge suspension) using a syringe and needle. The liquid was subjected to 0 kPa for 5 min followed by 20 kPa for 5 min. The cell was visually inspected for any sign of visible liquid penetration to the inside surface from the outside surface. At the end of the test, the challenge suspension was collected by opening the drain valve. The inside surface of the material (paper side) was washed with 5 mL of sterile nutrient broth, referred to as assay fluid. The entire surface area was brought into contact with the assay fluid by swirling the cell manually. If penetration was observed visually at any point earlier than the completion of the test, the cell was drained immediately and the assay fluid was collected and examined by viral titration using the soft agar overlay method with the media specified in the ISO 16604:2004 (E) protocol. The total number of plaques was counted. The sample passed the test if the count was less than 1 pfu/mL and vice versa. Positive and negative controls were performed using Whatman filter paper 602H and a heavy gauge polypropylene autoclavable bag material, respectively. All experiments were performed in triplicate.

Settle plates were performed to ensure there was no airborne contamination during any stage of the experiment. The agar plates containing *E. coli C* were exposed for 15–20 min at the locations of phage

titration and the penetration testing area. Material compatibility testing was performed to ensure there was no phage inactivation by the sample or the material of the penetration cell. This was done by pouring 10 mL of the phage suspension of 2200 pfu/ml onto the surface of the test material while it was in the cell. The lysate was then collected after 10 min of exposure to the sample and the cell. Phage titration was performed on this lysate as described above.

2.8. Ash content

The ash in the paper laminate composites were tested using the standard method TAPPI T211. Samples of known mass were combusted in an electrical muffle furnace (Model no. BT7670 Tetlow kilns & furnaces) at 525 °C for 3 h and the mass of the resulting ash was recorded. The moisture content was measured by keeping the samples of known mass in 105 °C for 4 h and recording the dried mass. The ash content was calculated as follows:

$$\text{Ash content } (\%) = \frac{\text{Weight of ash (g)}}{\text{Weight of paper sample (moisture free)(g)}} \times 100$$

3. Results

This study aimed to characterise laminated paper composite materials for their potential use as medical gown. The paper laminate composites were analysed by combining optical microscope and AFM-IR to detect surface composition and topographical heterogeneity of the base sheet-laminate interface, thus relating permeability to composite structure. The mechanical properties of the laminate materials, including tensile strength, seam strength and tear strength, were also analysed to quantify the effect of each layer. The materials were further tested against AAMI PB 70 for level 4 medical gowns, for which the required properties are >30 N for tensile and seam strength and >10 N for tear strength. The barrier properties of the composites were tested against both water and a bacteriophage virus to determine the role and importance of each layer.

3.1. Coating morphology

Laminate integrity is key in achieving the required level of viral protection. However, the PE coating must also be as thin as possible for economic purposes, and to optimise wearer comfort. Further, analysis of the level of adhesion and the morphology of the interface can reveal a new understanding of the diffusion and barrier properties of laminated papers. Here, we combine advanced optical microscopy with AFM-IR analysis to probe and quantify the surface and interface between the layers of laminated paper.

3.1.1. PE coating morphology visualised with optical microscopy and AFM-IR

The surface and interface between the layers of the laminated papers were measured through advanced optical microscopy combined with AFM-IR analysis (Fig. 1). The optical microscopy transmission (brightfield) image shows the underlying cellulose fibres while the reflectance image reveals coating morphology. Pinholes were not readily detectable in the brightfield images, but a faint hue of the dye was occasionally observed. The reflectance images show heterogeneous coating morphology across the samples. The images of the two thinnest laminate layers and base sheet thicknesses (B44/6 and B44/10) show light and dark domains, revealing higher amorphous arrangement of PE chains (dark) than the semi-crystalline domains (light), which is consistent with the AFM-IR observations (Fig. 2) [36]. Samples B44/15, B49/16 and 15/B49/16 show no distinct light and dark domains; however, an overall dense bubble morphology indicates air trapped in the melt.

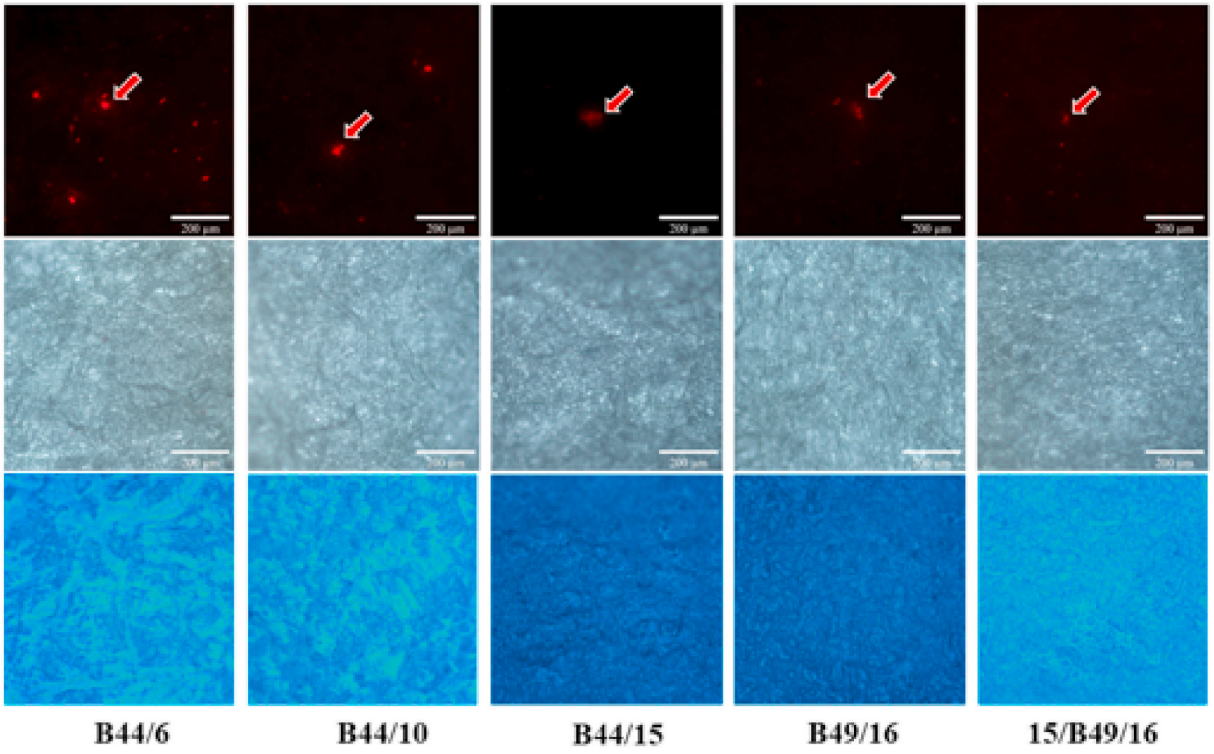

Fig. 1. Optical microscopy of laminate paper composites (scalebar: 200 μm) with PI staining. Fluorescence (top row), transmission (brightfield) (middle row) and reflectance with coloured filter (bottom row) images of propidium-iodide (PI) stained samples with various base sheet and laminate layer thicknesses. Fluorescence images reveal pinholes (in red), brightfield shows cellulose fibres and reflectance images highlight coating morphology. (For interpretation of the references to colour in this figure legend, the reader is referred to the Web version of this article.)

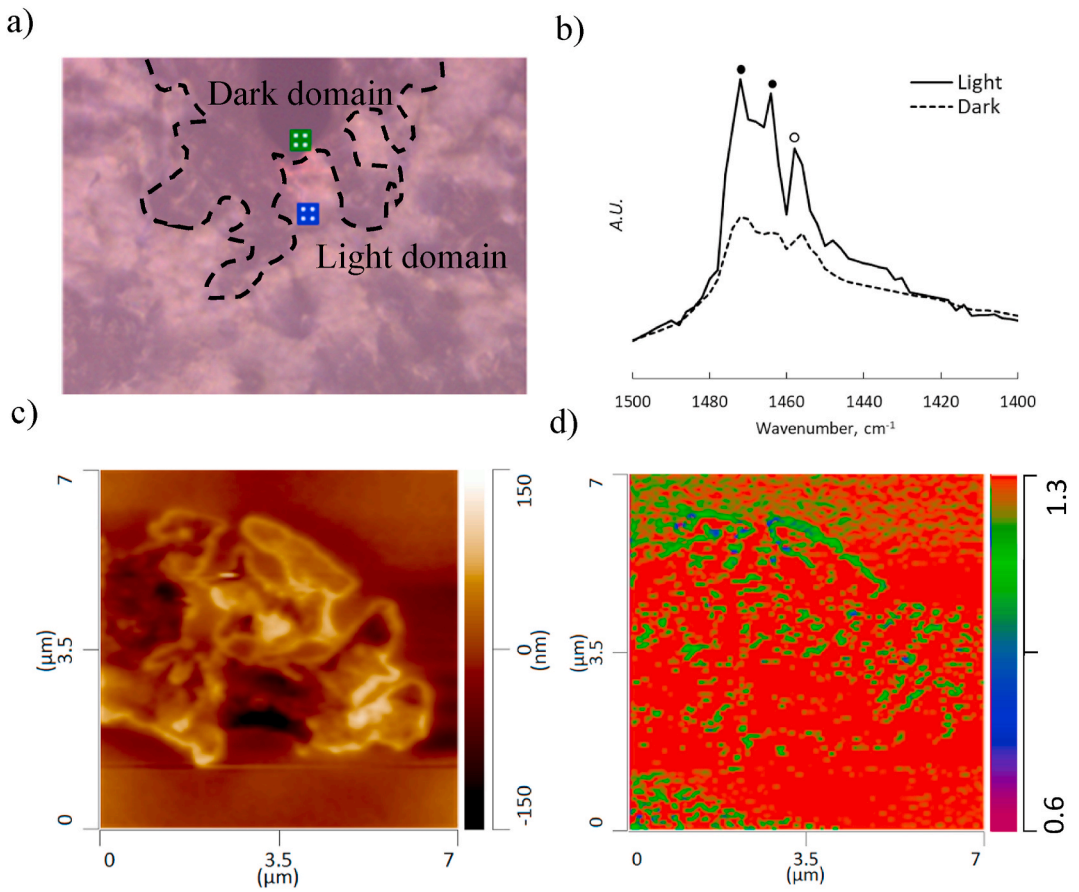

Fig. 2. Characterisation of the heterogeneous coating morphology of sample B44/10: a) NanoIR3 Optical microscopy view (375 × 282 μm) of the coating surface showing light and dark domains. b) AFM-IR spectrum showing the prominent CH_2 bending peaks of semicrystalline PE (solid circles, 1472 cm^{-1}, 1464 cm^{-1}) and amorphous PE (open circle, 1458 cm^{-1}). Dark domains have higher intensity due to semi-crystalline bands compared to the light regions, which show diminished semi-crystalline band signal intensity and similar intensity from the amorphous band. c) AFM topography map of a dark domain showing uneven surface morphology. D) PE (1464 cm^{-1}) -to-Cellulose (1062 cm^{-1}) IR ratio map of region (c) showing distinct PE rich (red) and PE poor (green) areas at the edges of the uneven surface topography. (For interpretation of the references to colour in this figure legend, the reader is referred to the Web version of this article.)

3.1.2. *Pinholes visualised with fluorescence microscopy and AFM-IR*

The fluorescence and optical images of selected samples after propidium iodide staining are displayed in Fig. 1. Fluorescence images show that the thinner laminate layer has the most pinholes while the thickest base sheet shows the least. The AFM topography images reveal two types of defect morphologies for pinholes. The first morphology is a protrusion of cellulose fibres through the coating from the base sheet due to insufficient amount of coating material (Fig. 3A); the other is a crater-like defect due to uneven coating (Fig. 3b). The AFM-IR shows an increase in the cellulose signal (1064 cm^{-1}) peak closer to the bottom of the crater-like defect than at shallower regions, indicating a thinner layer of the polyethylene coating at the base of the crater. The protruding fibre features give an even stronger cellulose signal at 1064 cm^{-1} in addition to a deformation of the polyethylene peak (1464 cm^{-1}) with lowered intensity and widened base. For protrusion defects, the IR composition map of polyethylene-to-cellulose ratio revealed poor polyethylene coating (Fig. 3c). A simultaneous measurement of the relative stiffness of the material was collected by tracking the resonant frequency of the AFM tip. The protruded defect generated higher frequencies than the surrounding area, indicating that a PE poor region can introduce mechanical heterogeneity, such as domains with high relative stiffness contrast compared to that of surrounding areas due to exposed cellulose material from base sheet (Fig. 3d).

3.2. *Mechanical properties*

Achieving the required mechanical properties with paper laminate materials, particularly high tensile strength, is expected to be challenging. Here, the effect of the type and thickness of paper base-sheet and the thickness of the PE coating are analysed. The material strength must also be preserved upon gown assembly, therefore two seam options, sewn and fused, are presented and analysed here.

3.2.1. *Tensile strength*

The mechanical properties of the laminated paper samples were expressed as the geometric mean tensile (GMT) at break point. Results are presented in Fig. 4. The dotted line represents the strength required (30N) for level 4 medical gown materials according to AAMI PB 70. All samples except the two newsprint composites meet the requirement. The newsprint composites (N42/10 and N51/10) have a lower GMT compared to those of bleached paper. These results indicate that pulp type plays an important role in governing the composite strength.

Increasing the thickness of the laminate for the same bleached base-sheet (B44/6, B44/10, B44/16) does not change the GMT significantly, nor does increasing the base sheet grammage from 44 to 49 GSM (B49/0 and B49/16). The effect of laminate thickness is also negligible when paper is coated on a single side. However, coating on both sides (15/B49/16) improves GMT significantly compared to single side coating.

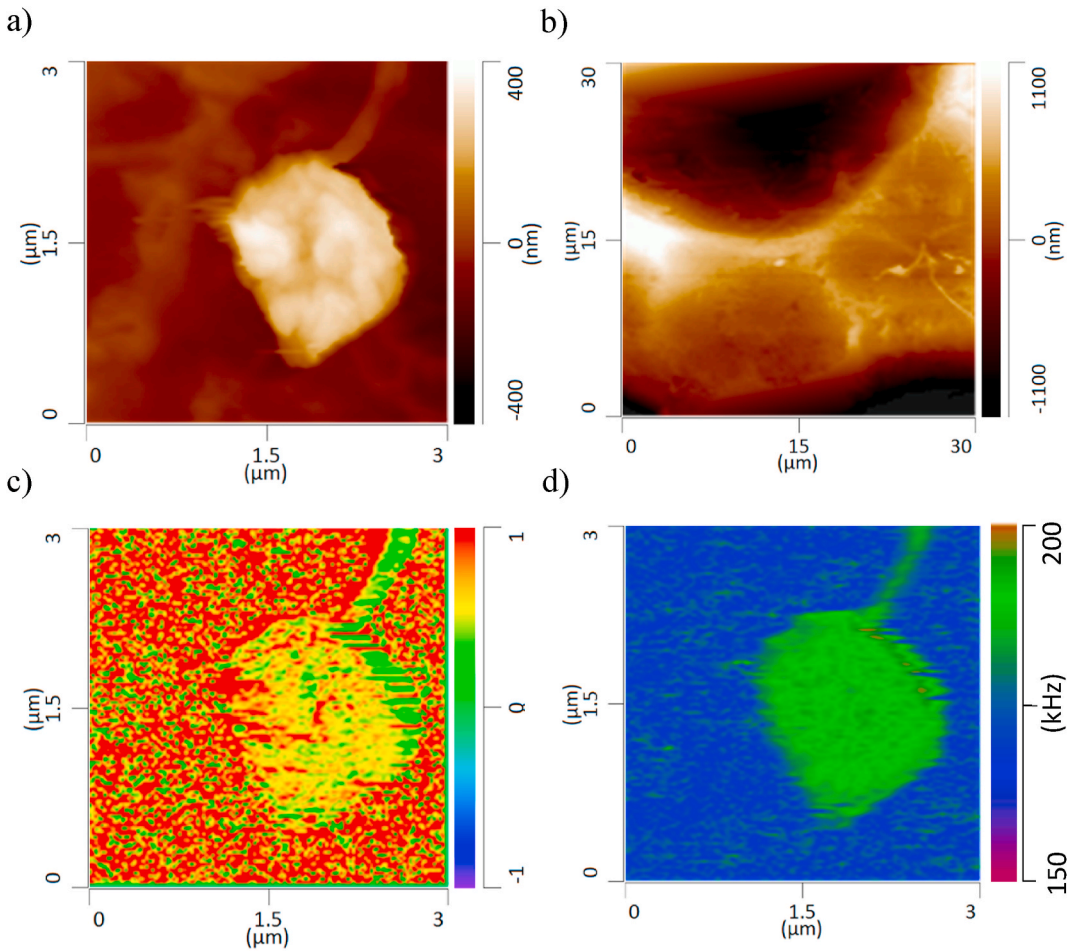

Fig. 3. Evidence of pinhole defect morphologies detected by AFM-IR characterization. a) An AFM topography map of a protruding defect (type 1) and b) An AFM topography map of a concave crater-like defect (type 2). c) PE (1464 cm^{-1}) -to-Cellulose(1062 cm^{-1}) IR ratio map of a protruding defect in A showing reduced IR absorption of 1464 cm^{-1} indicating poor PE coating on cellulose base sheet. d) PLL frequency map showing that protruding defects introduce domains with high relative stiffness contrast.

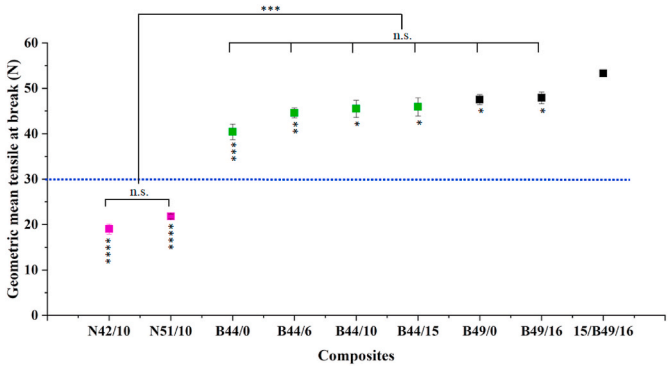

Fig. 4. Geometric mean tensile strength at break point for the different laminate composites. The dotted line shows the AAMI PB 70 requirement. The asterisks brackets show statistically significant differences between the indicated data points and groups. The asterisks below each data point show the level of significance when compared with 15/B49/16. Here, n.s. represents "not statistically significant", * represents $p \leq 0.05$, ** is for $p \leq 0.01$, *** for $p \leq 0.001$ and **** corresponds to $p \leq 0.0001$.

3.2.2. Seam strength

Seam strength was measured for both sewn and thermofused sample assemblies (Fig. 5). Slippage occurred for sewn seams at a low force for the unlaminated bleached paper with a 44 GSM base sheet (B44/0). Increasing the laminate thickness on this base sheet (B44/6, B44/10, B44/16) or increasing the base sheet grammage (B49/0) does not affect seam strength significantly. However, when higher GSM base sheets were laminated on one side (B49/16), the seam strength improved considerably. Coating the sample on both sides (15/B49/16) improves the seam strength compared to its single-sided laminated counterpart (B49/16). This material (15/B49/16) has significantly higher seam strength than the unlaminated base sheets (B44/0 and B49/0) and the laminated base sheet with a lower GSM (B44/6,10,15). Therefore, it appears that both base sheet and laminate layers contribute to seam strength.

Thermofused composites did not show any difference in seam strength, irrespective of base sheet grammage, laminate thickness, or double-sided coating. Moreover, none of the thermofused composites samples meet the seam strength required (30 N) for by AAMI PB 70 for level 4 medical gowns (Fig. 5b). However, the thermofuser used here was a kitchen heat seal and thus might not have provided sufficient heat.

3.3. Barrier properties

Paper laminate barrier properties are important to ensure protection from the surrounding environment. Here, the effect of the thickness of paper base sheet and the thickness of the coating are evaluated.

3.3.1. Water resistant

The water resistance of the composites was measured through

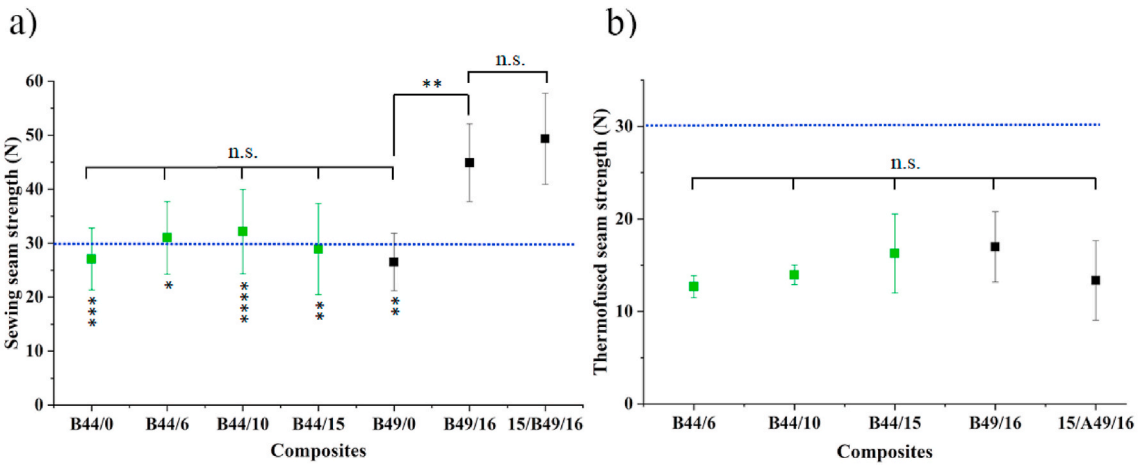

Fig. 5. Seam strength after (a) sewing and (b) thermofusing for the different laminate composites. The dotted line shows the AAMI PB 70 requirement. The asterisks brackets show statistically significant differences between data points and groups. The asterisks below each data point show the level of significance compared to 15/B49/16. Here, n.s. represents not statistically significant, * is $p \leq 0.05$, ** shows $p \leq 0.01$, *** for $p \leq 0.001$ and **** corresponds to $p \leq 0.0001$.

hydrostatic pressure and impact penetration tests with results displayed in Table SI and Fig. 6. The hydrostatic pressure increased with increasing base sheet thickness. However, a more substantial increase was observed when the effect of the laminate was considered simultaneously. For A44/0 and A49/0, hydrostatic pressure was 24 and 37 cm, respectively. These values increased above 98 cm when a coating layer was added.

Water penetration values decreased with increasing base sheet thickness. Similar to the hydrostatic pressure tests, the greatest impact was noted when a laminate layer was included. For A44/0 and A49/0, water penetration was 0.11 and 0.06 g, respectively, decreasing to below 0.3 g when a coating layer was added.

3.3.2. *Water vapour transmission rate*

Materials without a PE layer showed the highest water vapour transmission rate (WVTR) (Fig. 7). WVTR values were similar for different base sheet thickness (A44/0 and A49/0). However, introducing a PE layer to the base sheet decreased the WVTR by 94% for A44/6 (31.3 g/m^2.day) compared to the base sheet A44/0 (530.4 g/m^2.day). Increasing the laminate layer thickness further reduced the WVTR. The lowest WTVR (2.4 g/m^2.day) occurred when a laminate layer was applied to both sides of a base sheet (15/B49/16).

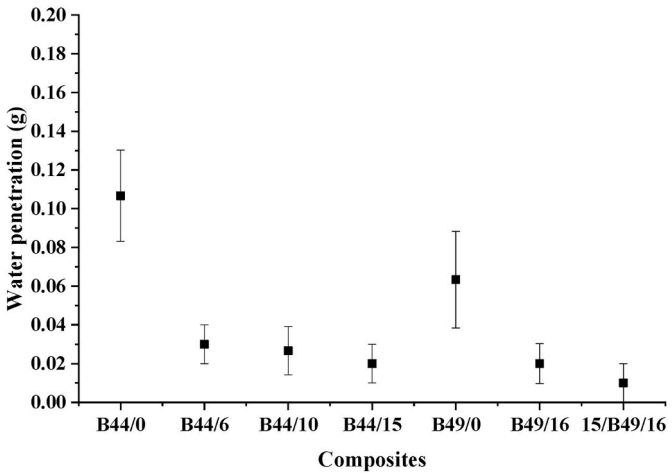

Fig. 6. Water penetration of the different samples.

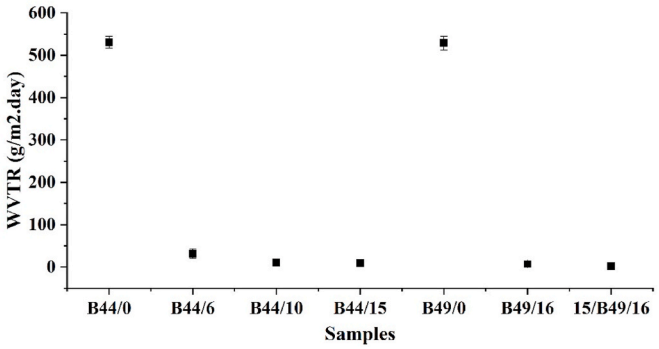

Fig. 7. Water vapour transmission rate for the different laminate composites.

3.4. *Virus protection*

The ability of the laminate materials to resist the penetration of viruses was tested using a surrogate virion Phi-X174 bacteriophage. The penetration of a virus suspension containing 10^7 pfu/mL from one side of the material to the other side was tested. Table S2 shows the resistance of the bleached paper samples coated with laminates of different thickness to virus penetration. The samples with a higher PE lamination passed the penetration tests irrespective of the paper type and base sheet grammage. The samples with low PE lamination (A44/6 and A44/10) failed the penetration test, whereas those with higher lamination (A44/15 and A49/16) could withstand a pressure of 20 kPa without allowing the virus particles to penetrate, thereby passing the test. The double coated sample (15/A49/16) also passed the test. The experimental method was validated with positive and negative controls. The positive control, which was a filter paper having a pore size of 2 μm, provided no barrier to the virus particles. The impermeable polyethylene material, with very low wettability and a small pore size, showed in no penetration of the virus suspension even under pressure.

Virus sizes usually range between 24 and 200 nm. The Phi-X174 bacteriophage tested here was reported to have an icosahedral shape with external spikes on each vertex, with a diameter of 25 nm excluding the spikes [37]. This virus particle is reported to be 34 ± 2 nm in size, including the spikes [38]. The viral species causing the COVID-19 outbreak is SARS-CoV-2. SARS-CoV-2 virions are spherical in shape, also containing glycoprotein spikes, and their diameter ranges from 60

nm to 140 nm [39,40]. SARS-CoV-2 viruses are larger than the microbe tested. It is therefore concluded that materials that provides barrier to the Phi-X174 bacteriophage would also resist penetration by the SARS-CoV-2 virus.

3.5. Ash content

The ash content signifies the presence of inorganic residues from wood pulp, the paper making process, and paper fillers. The ash content of the newsprint (N42/10) and bleached paper (B44/10) having the same laminate coating were 1.35 ± 0.36% and 0.50 ± 0.07%. The ash content of the newsprint sample was significantly higher than the bleached sample. The ash content of the uncoated bleached paper (B44/0) is 0.21 ± 0.12%, which shows that the 10 GSM coating also has some contribution to the ash.

4. Discussion

Paper based materials have never been reported for use as medical gowns. Thus, their prospect in this area remains poorly understood. At first, this material may seem to be an injudicious choice because of its perceived weakness, high porosity and high wicking ability. However, two events have challenged this perception. The first is the COVID crisis that has drastically limited access to typical polyolefin non-woven gown materials, which are predominantly manufactured in Asia [41,42]. In contrast, paper is manufactured on all the inhabited continents, and indeed, in most countries. The second is the advance of paper as an engineered material. Substantial progress in strength and barrier performance has been achieved in the last decade. However, commodity paper has yet to be reported as an accessible medical gown material, without the use of advanced technologies such as nanocellulose and assembling systems. This section has two objectives. The first is to investigate the property-structure relationship of laminated papers in the context of COVID-19 medical gown materials; the second is to determine if and how the current gown standard (AAMI PB 70) can be met with paper technology.

The AAMI PB 70 standard states the mechanical and barrier property requirements for medical gowns. Hence, these were studied to understand the suitability of the base sheet-laminate combination for Level 4 medical gowns, the highest level of protection. Special attention was dedicated to coating homogeneity, which was identified as a critical factor to ensure both reliability and safety of the material in COVID-19 medical gowns.

4.1. Material morphology

Defects in the laminate layer may compromise the barrier and mechanical function of laminated paper during use as COVID-19 surgical and isolation gowns. Due to the sub-micron size of the SARS-CoV-2 virus, a high resolution technique, namely AFM-IR, was utilised to acquire nanoscale structural and composition information regarding material defects by revealing these features with fluorescence staining. The concept is to stain the paper underneath the laminated surface with a fluorescent dye, which gives highly sensitive detection of any defects present.

Fluorescence stained regions, or pinholes, are defects which are more prevalent in composites with lower grammage base sheets, which introduces more pores in the sheet, or thinner laminate layers providing inadequate coverage over the rough paper surface. AFM-IR characterization reveals protruding (type 1) or crater like (type 2) defect morphologies with circular to ellipsoidal shapes that are 1–30 μm on the longest axis. Samples of the lowest base sheet grammage and thinner laminate layers (B44/6) have the largest type 1 and type 2 defects. The number of defects reduces with increasing laminate layer thickness (B44/15); in addition, an increase in base sheet grammage also aids in reducing the number and size of defects. The IR absorption of type 1 defects displays stronger absorptions around 1060 cm^{-1} and a reduced absorption around 1466 cm^{-1}. Type 2 defects exhibit an increase in absorption around 1060 cm^{-1} nearer the bottom of the crater. In addition, the relative stiffness of a type 1 defect is significantly higher than that of the surrounding material. This suggests protruding defects result from the base sheet having little to no coating while crater defects consists of regions with a thinner laminate layer with nano-holes at the bottom of the crater. Both types of defects must be mitigated as defects initiate tears and reduces barrier function, especially type 1 defects. However, mechanical and barrier test results must also be considered when determining the base sheet and laminate layer thicknesses (which determine the minimum number of defects) required for a functional yet economical medical gown.

AFM-IR analysis of light and dark domains visualised with optical microscopy reveals a heterogeneous coating morphology with distinct domains of semi-crystalline (light) and amorphous (dark) arrangement of polyethylene in materials with the lowest base sheet grammage (B44/6 and B44/10). While the nature of these domains does not indicate defects of the laminate layer, it does indicate reduced uniformity and molecular orientation, which may imply poor material function and impact laminate adhesion. Sollogoub et al. used optical microscopy to demonstrate that a substrate surface of higher roughness and lower polymer thickness had poor adhesion because the polymer had not reached the bottom of all the substrate surface irregularities due to the polymer flow being halted by crystallization or solidification [43]. Optical microscopy is thus a simple way to gauge the potential quality of laminate adhesion and to identify macroscopic coating defects.

4.2. Material performance

4.1.1. Effect of base sheet type

Two different types of base sheets were evaluated: Newsprint paper and Bleached Kraft paper. Newsprint paper is made from softwood pulp (yellow pine) by thermomechanical pulping, which involves refining (grinding) under saturated vapour to separate the fibres from wood [44] at temperatures above the glass temperature (T_g) of lignin. Newsprint paper retains most of its lignin and some of the hemicelluloses. In contrast, bleached Kraft paper is produced from hardwood (Eucalyptus) by chemical (Kraft) pulping, followed by bleaching. In Kraft pulping, wood chips are pre-steamed and mixed with a hot mixture of sodium hydroxide, sodium sulphide and water, which reacts with lignin to separate the cellulose fibres [45]. Around 90% of the lignin and most of the hemicelluloses are removed in this process. The chemical composition and wood polymer distribution of the two types of paper are thus significantly different. The most critically different properties are the length and therefore bonding abilities of the fibres with Pine fibres (L = 2 mm and D = 20 μm) being significantly coarser than Eucalyptus fibres (L = 0.8 mm, D = 8 μm).

The base sheet type directly affects strength, measured here as the maximum tensile force at rupture [46]. Composites made from Kraft-based paper are twice as strong (GMT) as bleached newsprint (N42/10 and N51/10). This is attributed to the high lignin content in the newsprint paper, which decreases fibre-fibre bonding by the limiting hydrogen bonding ability and reducing fibre conformability, resulting in a lower GMT. Wet end chemistry is not expected to play any significant role as only retention aids and sizing agents (internal and surface for Bleached Kraft paper) are used; there are no wet/dry strengths agents. Further, the Kraft paper contains no filler while the Newsprint likely contains some $CaCO_3$ from the recycling process. This supposition is supported by the ash content analysis, which shows that the newsprint composites (N42/10) has a higher ash content compared to the bleached Kraft paper (B44/10).

4.1.2. Effect of base sheet and laminate thickness

Virus penetration of these composites is entirely dependent on the laminate thickness; base sheet type and thickness has no effect. Samples

with thin laminate show penetration of the virus suspension from the outside (laminated) surface to the inside. A lower grammage base sheet (44 GSM) can provide full protection to virus particles only when the PE layer is above 15 GSM. Granzow et al. showed that gowns made of polypropylene resist fluid strikethrough and microorganism penetration better than those made of polyester or cotton [19]. Thus, it is the polymer coating on the laminated gowns that dictate the level of virus protection. Image analysis confirms that thinner laminates have a heterogeneous coating morphology, and defects may allow virus penetration. Coating thicknesses above 15 GSM show lower coating heterogeneity and less pinhole defects. Therefore, a thicker laminate coating should provide improved virus protection.

Increasing the laminate layer or base sheet thickness does not result in a statistically significant difference in the tensile strength. This is confirmed by the similar GMT results observed for the 44 GSM base sheet composite tested at three laminate layer thickness. The laminate layer mainly contributes to the flexibility or 'drapability' of the composite, and provides a hydrophobic barrier and viral barrier.

For seam strength, sewing outperforms thermofusing. Sewn seam slippage (displacement of thread) occurs at a low force for the unlaminated bleached paper and for laminated bleached papers with lower base sheet grammage. For the 44 GSM base sheets, increasing the laminate thickness does not affect the seam strength significantly. However, the seam strength improves significantly with laminated (one side) 49 GSM base sheets. Coating the sample on both sides further increases seam strength compared to unlaminated base sheets with the same grammage (B49/0). This indicates that both the base sheet and laminate layer contribute to seam strength. For the thermofused composites, increasing the base sheet thickness or the laminate thickness does not affect the seam strength, which is universally poor.

The presence of the laminate has a conspicuous effect on the barrier properties of the composites. The hydrostatic pressure of the paper composites significantly increases when a laminate layer is added, independent of the laminate thickness. Similar results are observed for water resistance and the water vapour transmission rate of laminated samples, which confirms that the polymer coating is responsible for the permeability and hydrophobicity of these composites [47].

4.1.3. Meeting standard requirements

16 GSM polyethylene lamination on a 49 GSM Kraft pulp base sheet is a suitable material for the production of Level 4 isolation gowns, as per the requirements of AAMI PB 70, providing the highest level of protection [10]. According to ASTM F3352-19, the laminated composite developed in this study meets the standard requirements for tensile and seam strength (matching or exceeding 30 N) [48]. The analysis indicates that the best combination is a 49 GSM base sheet with 16 GSM PE layer. Although the tear strength of all the laminated composites is lower than the standard requirement, this can potentially be improved by including a thin polypropylene (PP) layer between the composite base sheet and laminate layer, or with a tape or mesh at the ends, preventing crack propagation.

5. Conclusion

This study investigates polyethylene (PE) laminated paper as a novel material for the manufacture of disposable medical gowns meeting the stringent requirements for SARS-CoV-2 protection. Medical gowns have standards to meet in tensile strength, tear strength, seam strength, water penetration, hydrostatic pressure and viral protection.

Bleached and newsprint papers of varying basis weights were laminated with a polyethylene coating (on one or both sides). The laminated composites were characterised for coating morphology (optical microscopy and IR-AFM), mechanical properties, water resistance, water-vapour permeability and viral penetration. The performance achieved were compared to the medical gown material standards.

The water resistance of the laminated papers meets the standard requirements regardless of the laminate thickness or the base sheet grammage. The mechanical strength of the composite results from the type of paper base sheet, with bleached paper being the strongest. The virus protection is dependent on the laminate thickness; a minimum PE coating of 15 GSM is required for viral resistance, regardless of the paper base sheet. Image analysis of the laminated paper surface reveals coating heterogeneity in thinly coated laminates. A thicker coating is required for achieving a coating morphology free of defects, which is imperative for providing good viral protection. The laminated materials met all tensile and seam strength requirements; however, they failed the tear strength standard. A simple solution might be the addition of a tape or mesh at the ends, thus preventing crack propagation in paper. This research presented and validated PE laminated paper as a new material for medical gown and COVID-19 PPE equipment production.

Declaration of competing interest

The authors declare that they have no known competing financial interests or personal relationships that could have appeared to influence the work reported in this paper.

Acknowledgement

This project was supported by ARC Research Hub for Processing Advanced Lignocellulosics (PALS) and the Australian Pulp and Paper Technical Association (APPITA). The authors would also like to thank Norske Skog and Opal (formerly known as Australian Paper and Orora) for preparation of the composites in their mills. Many thanks to Adele Elice-Invaso (Executive Director, Appita), Frank Farchione (Market Development Manager, Amcor Functional Coatings), Russell Allan (Managing Director, Aurelia Group Consulting) and Howard Burvill (Technical Manager, Independent Consultant) for expertise and providing materials. Thanks to Mr. Long Hoh (Laboratory Manager, Department of Civil Engineer), Mr. John Rebolledo (Technical Officer, Department of Civil Engineer) and Mr. Ross Ellingham (Workshop Assistant, Department of Chemical Engineering) for helping out to prepare the experimental setup. Thanks to Monash Institute of Medical Engineering (MIME) for use of facilities.

Appendix A. Supplementary data

Supplementary data to this article can be found online at https://doi.org/10.1016/j.polymer.2021.123643.

References

[1] N.J. Rowan, J.G. Laffey, Challenges and solutions for addressing critical shortage of supply chain for personal and protective equipment (PPE) arising from Coronavirus disease (COVID19) pandemic - case study from the Republic of Ireland, Sci. Total Environ. 725 (2020) 138532.
[2] L. Vogel, Canada's PPE crisis isn't over yet, say doctors, Can. Med. Assoc. J. 192 (20) (2020) E563. E563.
[3] N. Shimasaki, M. Hara, R. Kikuno, K. Shinohara, A highly sensitive assay using synthetic blood containing test microbes for evaluation of the penetration resistance of protective clothing material under applied pressure, Biocontrol Sci. 21 (3) (2016) 141–152.
[4] F.S. Kilinc, A review of isolation gowns in healthcare: fabric and gown properties, J.Eng. fibres.Fabr 10 (3) (2015), 155892501501000313.
[5] Y. Guo, Y. Li, P.L. Wong, Environment and body contamination: a comparison of two different removal methods in three types of personal protective clothing, Am. J. Infect. Contr. 42 (4) (2014) e39–e45.
[6] Verbeek, J.H., B. Rajamaki, S. Ijaz, R. Sauni, E. Toomey, B. Blackwood, C. Tikka, J. H. Ruotsalainen, and F.S.K. Balci, Personal protective equipment for preventing highly infectious diseases due to exposure to contaminated body fluids in healthcare staff. Cochrane Database Syst. Rev., (4).2020.
[7] U.S. Food and Drug Administration, Enforcement policy for gowns, other aparel, and gloves during the coronavirus disease (COVID-19) public health emergency, in: U.S.D.o.H.a.H. Services, United States of America, 2020.
[8] Administration, U.S.F.D. Medical gowns [cited 2020 27 May]; Available from: https://www.fda.gov/medical-devices/personal-protective-equipment-infection-control/medical-gowns, 2020.

[9] F.S.K. Balci, Isolation gowns in health care settings: laboratory studies, regulations and standards, and potential barriers of gown selection and use, Am. J. Infect. Contr. 44 (1) (2016) 104–111.

[10] A.A.M.I. PB70, Liquid barrier performance and classification of protective apparel and drapes intended for use in health care facilities, Association for the Advancement of Medical Instrumentation, Arlington (VA), 2012.

[11] Association for the Advancement of Medical Instrumentation, Selection and use of protective apparel and surgical drapes in health care facilities, Technical Information Report: TIR11: 2005 (2005).

[12] E. Bowden, C. Campanile, B. Golding, Worker at NYC Hospital where Nurses Wear Trash Bags as Protection Dies from Coronavirus. New York Post, 2020.

[13] Coronavirus BBC, UK Failed to Stockpile Crucial PPE, in BBC, 2020 (United Kingdom).

[14] Ford Ramps up PPE Production amidst Collaboration with Thermo Fisher on COVID-19 Test Kits, in Legal Monitor Worldwide, 2020. NA.

[15] HanesBrands, HanesBrands begins production of medical gowns in addition to cloth face coverings to supplement personal protection supply during COVID-19 pandemic, in: Medical Letter on the CDC & FDA, 2020, p. 1342. Atlanta.

[16] From Sanitizer to Gloves to Gowns, Wisconsin Company Vonco Steps up to Combat COVID-19 in America, in Plus Company Updates, 2020. NA.

[17] Dow, Partners to develop and donate level 2 medical isolation gowns, in: M2 Pharma, NA, 2020.

[18] PPE company starts production of reusable gowns, coveralls in response to COVID-19, in: Legal Monitor Worldwide, NA, 2020.

[19] J.W. Granzow, J.W. Smith, R.L. Nichols, R.S. Waterman, A.C. Muzik, Evaluation of the protective value of hospital gowns against blood strike-through and methicillin-resistant Staphylococcus aureus penetration, Am. J. Infect. Contr. 26 (2) (1998) 85–93.

[20] T. Dargaville, K. Spann, M. Celina, Opinion to address a potential personal protective equipment shortage in the global community during the COVID-19 outbreak, Polym. Degrad. Stabil. (2020) 109162.

[21] M.A. El-Samahy, S.A.A. Mohamed, M.H. Abdel Rehim, M.E. Mohram, Synthesis of hybrid paper sheets with enhanced air barrier and antimicrobial properties for food packaging, Carbohydr. Polym. 168 (Supplement C) (2017) 212–219.

[22] M. Maliha, M. Herdman, R. Brammananth, M. McDonald, R. Coppel, M. Werrett, P. Andrews, W. Batchelor, Bismuth phosphinate incorporated nanocellulose sheets with antimicrobial and barrier properties for packaging applications, J. Clean. Prod. 246 (2019).

[23] G. Rodionova, M. Lenes, Ø. Eriksen, Ø. Gregersen, Surface chemical modification of microfibrillated cellulose: improvement of barrier properties for packaging applications, Cellulose 18 (1) (2011) 127–134.

[24] L. Mendoza, L. Hossain, E. Downey, C. Scales, W. Batchelor, G. Garnier, Carboxylated nanocellulose foams as superabsorbents, J. Colloid Interface Sci. 538 (2019) 433–439.

[25] M.N. Alam, L.P. Christopher, Natural cellulose-chitosan cross-linked superabsorbent hydrogels with superior swelling properties, ACS Sustain. Chem. Eng. 6 (7) (2018) 8736–8742.

[26] A.M.A. Hasan, M.E.-S. Abdel-Raouf, Cellulose-based superabsorbent hydrogels, in: M.I.H. Mondal (Ed.), Cellulose-Based Superabsorbent Hydrogels, Springer International Publishing, Cham, 2019, pp. 245–267.

[27] R.M. Barajas-Ledesma, A.F. Patti, V.N.L. Wong, V.S. Raghuwanshi, G. Garnier, Engineering nanocellulose superabsorbent structure by controlling the drying rate, Colloid. Surface. Physicochem. Eng. Aspect. 600 (2020) 124943.

[28] G. Metreveli, L. Wågberg, E. Emmoth, S. Belák, M. Strømme, A. Mihranyan, A size-exclusion nanocellulose filter paper for virus removal, Advanced Healthcare Materials 3 (10) (2014) 1546–1550.

[29] A. Onur, A. Ng, G. Garnier, W. Batchelor, Engineering cellulose fibre inorganic composites for depth filtration and adsorption, Separ. Purif. Technol. 203 (2018) 209–216.

[30] A. Basu, G. Celma, M. Strømme, N. Ferraz, In vitro and in vivo evaluation of the wound healing properties of nanofibrillated cellulose hydrogels, ACS Applied Bio Materials 1 (6) (2018) 1853–1863.

[31] E. Caló, V.V. Khutoryanskiy, Biomedical applications of hydrogels: a review of patents and commercial products, Eur. Polym. J. 65 (2015) 252–267.

[32] M. Jorfi, E.J. Foster, Recent Advances in Nanocellulose for Biomedical Applications, 2015 n/a-n/a.

[33] AATCC TM42-2017e, *Test Method for Water Resistance: Impact Penetration test*, AATCC, North Carolina, USA, 2017.

[34] AATCC TM127-2018, *Test Method For Water Resistance: Hydrostatic Pressure*, North Carolina, 2018.

[35] N. Bonilla, M.I. Rojas, G. Netto Flores Cruz, S.H. Hung, F. Rohwer, J.J. Barr, Phage on tap-a quick and efficient protocol for the preparation of bacteriophage laboratory stocks, PeerJ 4 (2016), e2261.

[36] H. Hagemann, R. Snyder, A. Peacock, L. Mandelkern, Quantitative infrared methods for the measurement of crystallinity and its temperature dependence: polyethylene, Macromolecules 22 (9) (1989) 3600–3606.

[37] K. Yazaki, Electron microscopic studies of bacteriophage phi X174 intact and "eclipsing' particles, and the genome by the staining, and shadowing method, J. Virol Methods 2 (3) (1981) 159–167.

[38] M.E. Bayer, R.W. DeBlois, Diffusion constant and dimension of bacteriophage phi X174 as determined by self-beat laser light spectroscopy and electron microscopy, J. Virol. 14 (4) (1974) 975–980.

[39] N. Zhu, D. Zhang, W. Wang, X. Li, B. Yang, J. Song, X. Zhao, B. Huang, W. Shi, R. Lu, P. Niu, F. Zhan, X. Ma, D. Wang, W. Xu, G. Wu, G.F. Gao, W. Tan, A novel coronavirus from patients with pneumonia in China, 2019, N. Engl. J. Med. 382 (8) (2020) 727–733.

[40] Y.M. Bar-On, A. Flamholz, R. Phillips, R. Milo, SARS-CoV-2 (COVID-19) by the numbers, eLife 9 (2020), e57309.

[41] J.M.R. Andrew, B. Mike, At war with no Ammo: doctors say shortage of protective gear is drive, in: The New York Times, The New York Times, New York, 2020.

[42] The Food and Drug Administration, FAQs on shortages o surgical masks and gowns during the COVID-19 Pandemic [cited 2020 5/11/2020]; Available from: https://www.fda.gov/medical-devices/personal-protective-equipment-infection-control/faqs-shortages-surgical-masks-and-gowns-during-covid-19-pandemic, 2020.

[43] C. Sollogoub, P. Montmitonnet, Y. Demay, J.-F. Agassant, P. Deparis, Origin of the bubble defect in the extrusion coating process, Polym. Eng. Sci. 51 (2) (2011) 347–357.

[44] Skog Norske, Newsprint [cited 2020 1/10/2020]; Available from: https://www.norskeskog.com/Products/Newsprint, 2020.

[45] J. Fernández-Rodríguez, X. Erdocia, F. Hernández-Ramos, M.G. Alriols, J. Labidi, Lignin separation and fractionation by ultrafiltration, in: Separation of Functional Molecules in Food by Membrane Technology, Elsevier, 2019, pp. 229–265.

[46] A. TUTU, U. YILMAZ, M. ÇĢÇEKLER, *Effects of physical Properties of some Papers on offset printing quality*, in *IV*, in: International Multidisciplinary Eurasian Congress, 2017. Rome-Italy.

[47] P.W. Klein, in: Morgan, P. Claypool (Eds.), Fundamentals of Plastics Thermoforming, San Rafael, Calif.: San Rafael, Calif, Morgan & Claypool Publishers, 2009.

[48] F3352-19, A., Standard Specification for Isolation Gowns Intended for Use in Healthcare Facilities, ASTM International, West Conshohocken, PA, 2019.